ELSEVIER

Journal of Fluids and Structures 25 (2009) 641–653

JOURNAL OF FLUIDS AND STRUCTURES

www.elsevier.com/locate/jfs

Insights on vortex-induced, traveling waves on long risers

J. Kim Vandiver*, V. Jaiswal, V. Jhingran

Department of Mechanical Engineering, Massachusetts Institute of Technology, 77 Massachusetts Avenue, Room 5-222, Cambridge, MA, USA

Received 14 April 2008; accepted 12 November 2008
Available online 16 April 2009

Abstract

This paper is based on portions of a keynote presentation, which explored the boundaries of what is understood about the vibration behavior of long cylinders excited by vortex shedding. The source of data is a recent field experiment on a long flexible cylinder, densely instrumented with fiber optic strain gauges. The paper emphasis is on previously unknown or unexplained phenomena and in some cases offers provocative insights as opposed to conclusive proofs. Three particular topics are covered: (i) the occurrence of peak strain and fatigue damage rates at unexpected locations, (ii) the dominance of traveling wave rather than standing wave response, and (iii) the appearance of stable cylinder trajectories, such as figure eights and crescents in pure traveling wave regions. Potential explanations are offered and areas for promising additional research are proposed.

Keywords: Vortex-induced vibration (VIV); Traveling waves; Fatigue damage

1. Introduction

In the summer of 1981, a 22 m long steel pipe was stretched between pilings and exposed to a uniform tidal current. The expected flow-induced vibration was clearly evident in third mode, cross-flow (CF) standing waves, locked in synchrony with the formation of the wake. The unexpected surprise was the large amplitude, double frequency, in-line (IL) motion in the fifth mode, which was phase-locked to the CF motion, resulting in beautiful crescent and figure-eight-shaped trajectories (Vandiver, 1993). Only recently detailed hydrodynamic explanations have been given for such motions, based on laboratory experiments with spring-mounted rigid cylinders and for first mode standing wave vibrations of flexible cylinders (Dahl, 2008; Dahl et al., 2007; Jauvtis and Williamson, 2004). The same experiments have also provided some insight on the hydrodynamic causes of higher harmonic forces on cylinders. Recently, the authors conducted experiments on very long flexible cylinders in the ocean. These experiments have revealed the unexpected dominance of traveling waves with strong higher harmonic components and stable figure eight trajectories (Jaiswal and Vandiver, 2007; Jhingran, 2008; Jhingran and Vandiver, 2007; Marcollo et al., 2007; Swithenbank and Vandiver, 2007). Although some new unexpected response behavior was observed, the observations are consistent with the lessons learned from the laboratory experiments.

*Corresponding author. Tel.: +1 617 253 4366; fax: +1 617 258 5288.
E-mail address: kimv@mit.edu (J.K. Vandiver).

0889-9746/$ - see front matter © 2008 Elsevier Ltd. All rights reserved.
doi:10.1016/j.jfluidstructs.2008.11.005

2. Experiment description

Two field experiments were conducted by MIT and the Deepstar Consortium in 2004 and 2006. These experiments provided spatially dense measurements of high mode number response of flexible cylinders to vortex-induced vibration (VIV). The experiments were conducted in and near the Gulf Stream from the Research Vessel, Walton Smith, operated by the University of Miami. The experiments are referred to as Miami I (2004) and Miami II (2006) and were described in references Jaiswal and Vandiver (2007), Jhingran and Vandiver (2007), and Swithenbank and Vandiver (2007). The data used in this paper come from the Miami II experiment, which made use of a fiber glass composite pipe 500.4-foot-long (152.4 m) and 1.43 in (3.63 cm) in outer diameter. A railroad wheel weighing 805 lbs in air, 725 lbs (3225 N) in water, was attached to the bottom of the pipe to provide tension. A diagram of the experiment configuration is shown in Fig. 1. Dry weight of the pipe = 0.517 lb/ft (0.7694 kg/m), dry weight plus trapped water = 0.8522 lb/ft (1.2682 kg/m). The specific gravity of the pipe including trapped water was 1.1864. The submerged weight per unit length was 0.1385 lb/ft (2.021 N/m). A new measurement technology, fiber optic strain gauges, provided the capability to measure both IL and CF motions with a spatial resolution of 7 ft (2.133 m). Eight optical fibers were embedded in the outer layers of the composite pipe. Each fiber contained 35 strain gauges, which used the principle of Bragg diffraction to measure strain with a resolution of approximately 1 micro-strain. Pairs of fibers were spaced in four quadrants

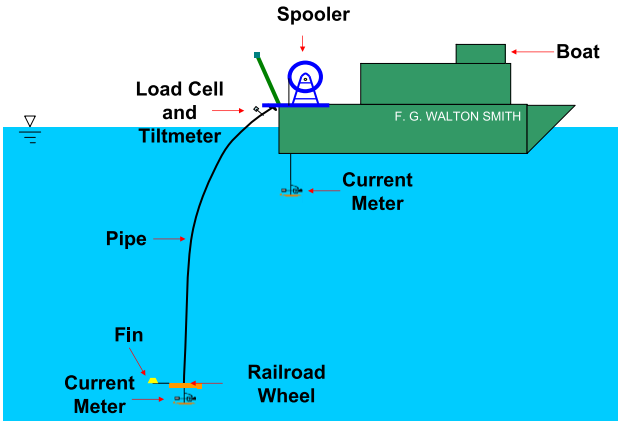

Fig. 1. Set-up for the Gulf Stream experiments 2006.

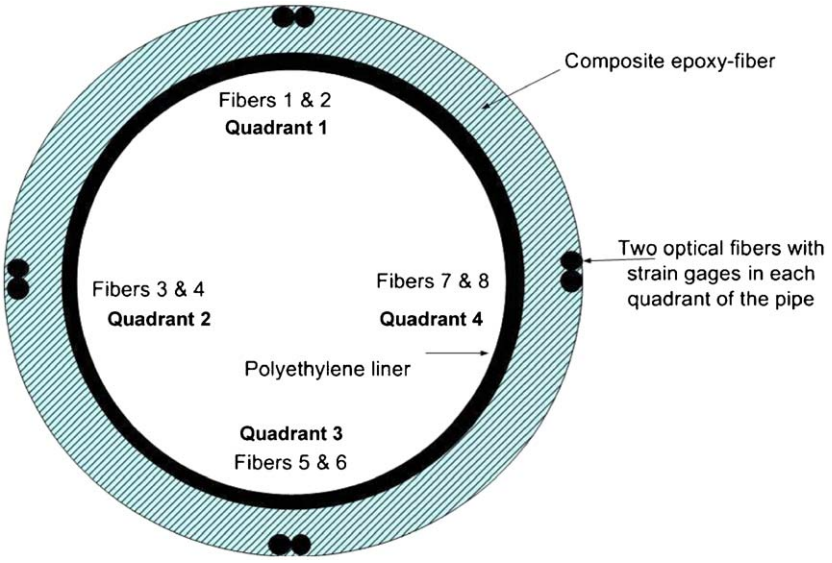

Fig. 2. Cross-section of the pipe.

at 90° intervals around the circumference of the pipe as shown in Fig. 2. Due to twist in the pipe, the fibers and gauges were usually not aligned with the CF or IL direction. As a result, the gauges in all the quadrants would typically reveal components of both CF and IL vibrations. The total CF and IL strain components can be isolated by appropriate vector computations.

The R/V F.G. Walton Smith is equipped with two acoustic Doppler current profilers (ADCPs). During the experiments, the ADCP was used to record the current velocity and direction along length of the pipe. Additional instrumentation included a tilt meter to measure the inclination at the top of the pipe, a load cell to measure the tension at the top of the pipe, a pressure gauge to measure the depth of the railroad wheel and two mechanical current meters to measure current at the top and the bottom of the pipe.

The boat was put on various headings relative to the Gulf Stream so as to produce a large variety of currents, varying from nearly uniform to highly sheared in speed and direction. At a typical VIV frequency of 4 Hz, this provided approximately five strain measurements per vibration wave length in the CF direction. The sampling frequency was approximately 50.48 Hz, which was sufficient to allow observation of vibration at up to five times the fundamental vortex shedding frequency. For the purposes of this paper, the fundamental vortex shedding frequency will be referred to as the $1\times$ or one times frequency. The higher harmonics will be referred to as the $2\times$, $3\times$, $4\times$, and $5\times$ higher harmonics. The $1\times$ vibration is the typical CF vibration response frequency associated with vortex shedding. The $3\times$ and $5\times$ vibration components are also associated with the CF motion, while the $2\times$ and $4\times$ components are characteristic of the IL vibration. The $2\times$ response is the common IL response at twice the CF vibration frequency.

The use of strain gauges favored the observation of the higher harmonics because for a given displacement amplitude, the curvature and hence the measured strain increases in proportion to the square of the vibration frequency. Therefore, even rather small amplitude higher harmonic waves result in strain amplitudes that are of magnitude comparable to the strain associated with the $1\times$ CF vibration.

3. A typical example of measured response

When the pipe was towed through still water, the resulting VIV was, as expected, very energetic. Fig. 3(a) shows the speed of one of the more uniform current profiles. In this case the direction was uniform. The angle of the pipe relative to vertical is zero at the bottom and increases monotonically toward the top due to accumulating mean drag force.

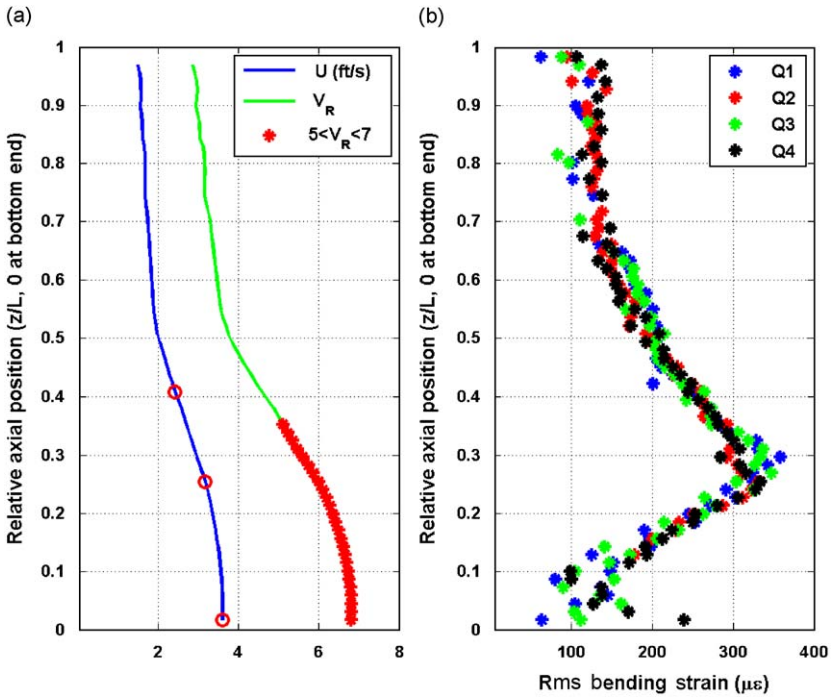

Fig. 3. (a) Measured current speed and reduced velocity. (b) Measured rms quadrant bending strain.

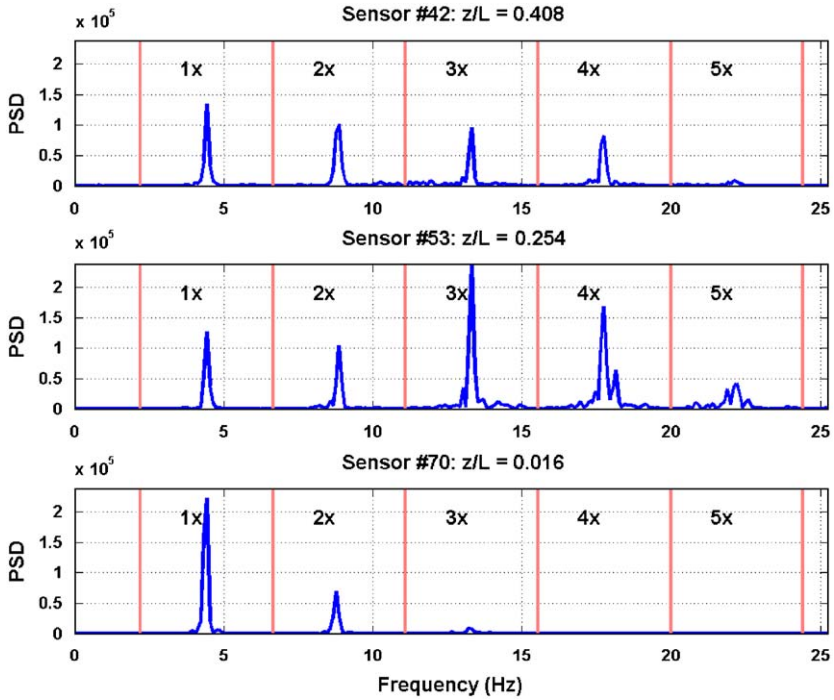

Fig. 4. Spectra at three different locations.

At the higher test speeds the top angle often exceeded 45°. The current speed shown is the velocity component perpendicular to the pipe, which diminishes near the top due to the increasing slope. The spatial average of the standard deviation of the local current speed estimate was 0.11 ft/s. Fig. 3(a) also shows the local reduced velocity, defined as $V_R = U/f_v D$, where D is the pipe outer diameter, U is $U(z)$, the local current speed and f_v is the peak $1\times$ response frequency in the source excitation region. Over a wide range of cases the source of the pipe VIV was associated with regions of the pipe with reduced velocity in the range of 5–7. This zone is shown in red on the reduced velocity curve in Fig. 3(a)—the lower part of the curve. The spatial average of the standard deviation of the local reduced velocity estimate was 0.20. The total rms bending strain response in all the four quadrants (labeled Q1–Q4) is shown in Fig. 3(b). The effect of low frequency vessel motion (below 1 Hz) has been removed from the strain data by high-pass filtering it.

Fig. 4 shows the spectra of response at three different axial locations, with z/L coordinates of 0.016, 0.254, and 0.408, where $z/L = 0$ is at the bottom end. These locations are shown in Fig. 3(a) with red circles on the current profile. In each case the spectra are the sum of the spectra of two orthogonal gauges at each elevation. Hence all IL and CF frequency components will be revealed in the spectra. The top or first spectrum of the three shown is at $z/L = 0.408$, which places it about fifteen meters above the location of maximum rms response as shown in Fig. 3(b). All of the response harmonics are represented in the spectrum. The $1\times$ peak frequency is at 4.44 Hz, which corresponds to a wavelength of approximately 32 ft (9.3 m).

The spectrum measured at $z/L = 0.254$ also has peaks at all harmonics, with an especially large $3\times$ peak. In contrast, the spectrum from $z/L = 0.016$ has $1\times$ and $2\times$ peaks but almost negligible $3\times$, $4\times$, and 5X peaks. This indicates that there is little $3\times$, $4\times$, and $5\times$ harmonic response close to the boundary. At $z/L = 0.016$, the location of the sensor closest to the boundary, the measurement point is very close to an anti-node (maximum) of vibration for a $1\times$ standing wave at 4.44 Hz and near a node for a $2\times$ standing wave. Both displacement and strain have maxima and minima at the same location when the structure vibrates in standing or sinusoidal traveling waves.

4. Unexpected features of the dynamic response

The location and character of peak response. Prior to these experiments, the accepted explanations and models for VIV excitation would have led one to expect a large standing wave region near the bottom end boundary and associated with

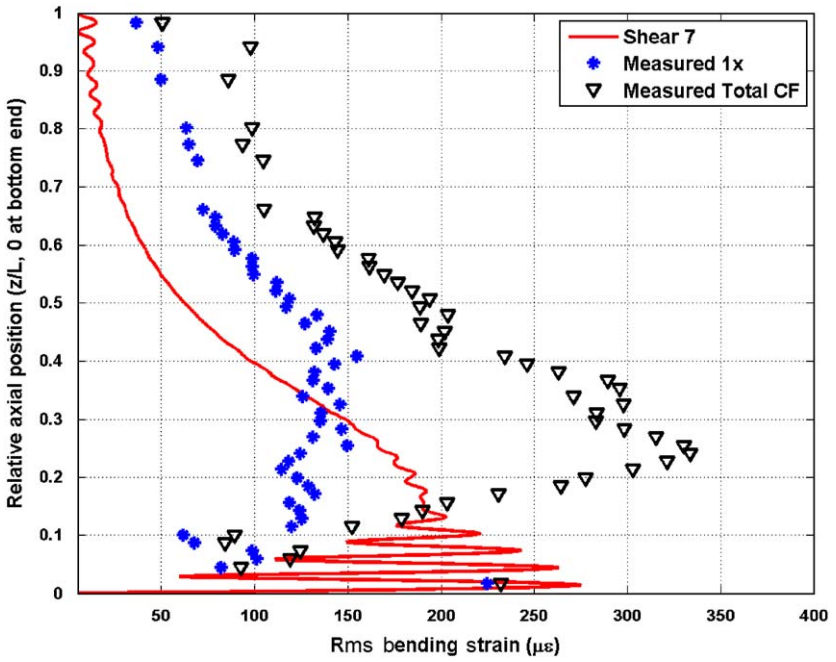

Fig. 5. Shear7 predicted strain response, measured $1\times$ strain component and measured total cross-flow (CF) strain.

a reduced velocity range of approximately 5–7. Fig. 5 shows a SHEAR7[1] prediction of the $1\times$, rms strain response for the Miami II riser, exposed to the current profile given in Fig. 3(a). It predicts a standing wave which increases in amplitude, as one approaches the bottom end, with the peak rms CF strain occurring at one quarter of a wavelength (2.44 m) from the bottom boundary. Fig. 5 also shows the measured total rms CF strain and the measured $1\times$ component. The total rms peaks far from the boundary. The $1\times$ component peaks near the boundary, but is much smaller than expected.

Figs. 6(a) and (b) show the measured rms total CF and total IL strain responses as a function of the dimensionless axial coordinate, z/L, measured upward from the weight at the bottom end. The response has been high-pass filtered at 1 Hz to remove strain caused by vessel motion. All functioning sensors are shown. The peak rms CF response is at $z/L = 0.25$ and the IL is at $z/L = 0.30$. This seems to contradict the expectation that the response should be highest near the boundary due to the expected standing wave pattern. A part of the explanation is made clear in Figs. 6(a) and (b), which also show the rms strain caused by each harmonic. The $1\times$ contribution does in fact have its maximum at $z/L = 0.016$ and is the result of the standing wave near the boundary. SHEAR7 only predicts the $1\times$ component, and in this case agrees with the location, but over predicts the magnitude of the $1\times$ strain. The $3\times$ and $5\times$ contributions have peak response away from the boundary. This causes the total rms response to have a peak at $z/L = 0.25$. In the IL direction, the RMS $2\times$ response is large from $z/L = 0.20$ to 0.40 and the $4\times$ component peaks at 0.30. The explanation for why the higher harmonics do not peak near the boundary must wait for the traveling wave discussion.

The dominance of traveling wave response. Traveling wave dominance was not expected, but when the response was plotted as shown in Fig. 7, the evidence was undeniable. Fig. 7 shows the $1\times$, time domain contribution to the total response in the CF direction at all 70 response locations in one of the quadrants. The horizontal axis is the passage of time in seconds. The vertical axis, z/L, is the non-dimensional axial location on the riser from bottom ($z/L = 0$) to top ($z/L = 1$). The time series at each location were filtered to reveal only the vibration at the fundamental $1\times$, CF response frequency. The color of the plot indicates the instantaneous amplitude of the measured strain. For example, red indicates a strong positive strain (top of color bar), while blue (bottom) indicates strong negative strain. If one scans horizontally across the figure at, for example, $z/L = 0.3$, one sees alternating red and blue which indicates that at that location the strain gauge measured an oscillation in strain at the $1\times$ frequency of 4.44 Hz. As one scans the figure

[1]SHEAR7 is an industry standard program used for VIV and fatigue life prediction of risers.

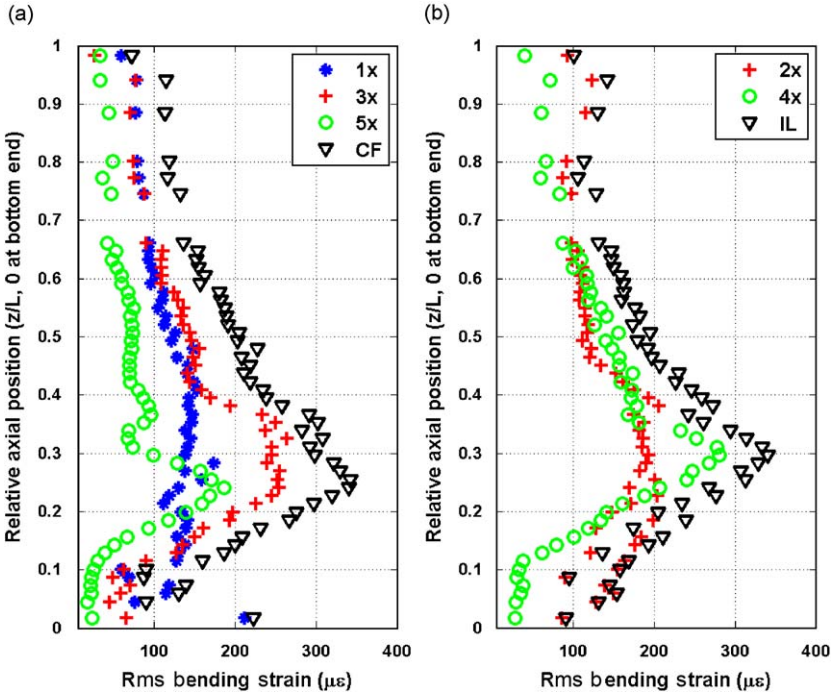

Fig. 6. Strain components. (a) Cross-flow (odd harmonics). (b) In-line (even harmonics).

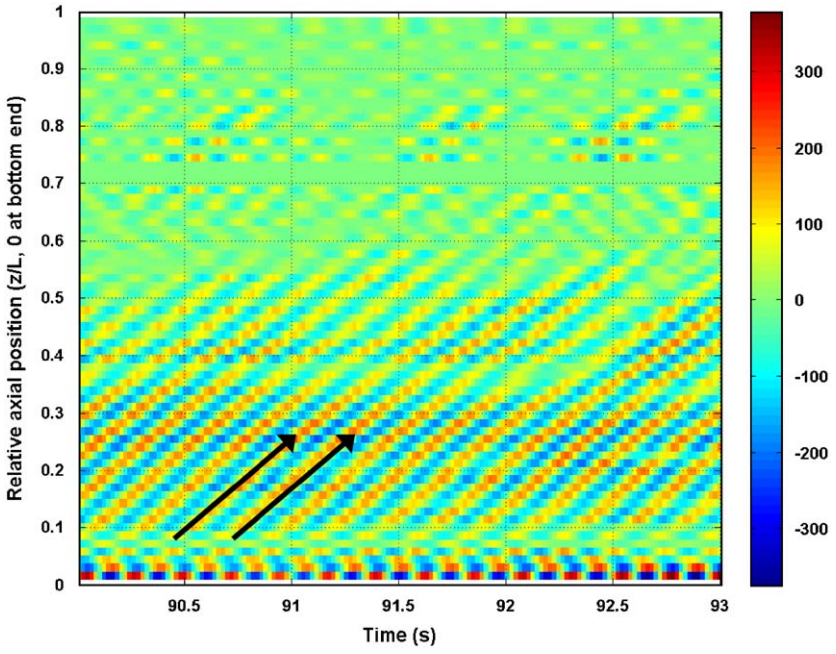

Fig. 7. $1\times$ strain time series at all sensor locations showing traveling wave behavior with speed approximately 40 m/s. The arrows in the figure indicate how crests travel in space and time.

vertically from $z/L = 0.1$ to 0.7, diagonal rows of constant color are quite conspicuous. These are the crests of bending waves racing up the riser. From the slope of the diagonal rows, the propagation speed may be estimated at approximately 40 m/s.

Although it was not possible in these field experiments to make observations of the wake behind the cylinder, such figures are strong evidence that the traveling waves are created by lift forces due to vortex shedding which is phase locked to the traveling wave. If one could visualize the wake, one would see vortex trails being shed obliquely in the flow and not parallel to the axis of the cylinder. The vortices in the wake, if visible, would look much the same as does the plotted strain in this figure. In other words, for every bending wave crest moving up the riser, there is a vortex street separating from the cylinder and the point of separation is moving up the pipe at 40 m/s.

Conventional wisdom prior to the experiments had been that while towing in still water, the power-in region would be a standing wave pattern with largest amplitude near the weight at the bottom end. This standing wave region would be a region where the vortex shedding process was synchronized or locked-in to the motion of the cylinder. This region was expected to have a variation in reduced velocity of approximately 5 to 7, which for this example would have extended from $z/L = 0.0$ to $z/L = 0.36$ as shown in the plot of reduced velocity in Fig. 3(a). Such a locked-in region would have been 5.5 wavelengths long at 4.44 Hz. It was also expected that traveling waves would exit the power-in region and travel up the pipe, decaying in amplitude as they progressed.

What one can see in Fig. 7 is a standing wave region, starting at the bottom boundary and persisting to $z/L = 0.10$, which is about 15 m in length (1.5 wavelengths). It is less energetic than expected. Above that region is a long traveling wave region in which the wave amplitudes increase as they progress up the pipe, rather than decay as had been expected. It is the increase in vibration energy with distance from the bottom end that shows that the vortex shedding forces are amplifying the bending waves as they travel up the pipe. Eventually the excitation region ends and the traveling wave amplitudes begin to decay with further travel up the pipe. The end of the traveling wave excitation region corresponds approximately to a reduced velocity of 5.0 which occurs at $z/L = 0.36$. Before attempting an explanation for this behavior, it is useful to describe the third surprising phenomena.

The appearance of stable figure eight trajectories in traveling wave regions. This paper began with a description of figure eight trajectory motion of a pipe exhibiting third mode standing wave lock-in and fifth mode IL resonance. The pipe had significant bending stiffness. Several very special conditions had to be simultaneously satisfied in order to enable the observed motion. It was with considerable astonishment that similar motion such as that shown in Fig. 8, was observed in the Miami II data (Jhingran, 2008). This figure is a plot of 3 s of strain data for all sensor locations in the bottom half of the pipe. At each location the time series of CF motion is plotted against the IL, yielding trajectories of the motion at that location. The time series of the CF has been filtered to isolate the $1\times$ component and in the IL direction the times series has been filtered to isolate the $2\times$ component. The IL strain component has been divided by four to remove the wavenumber-squared amplification. In other words the resulting plots are proportional to the plots that would result from plotting CF versus IL displacement.

From $z/L = 0.0$ to 0.10 the trajectories change rapidly. From $z/L = 0.10$ to 0.20 the motion remains in a figure of eight. This is a distance of approximately one and a half wavelengths and is entirely in a traveling wave region. In this range the motion is known to be increasing in amplitude as can be seen in the rms plots, as is shown in Figs. 6(a) and (b). From 0.20 to 0.42 the trajectories go through substantial variation and then settle down again to a long region of crescent-shaped trajectories from $z/L = 0.42$ onwards. In this region the crescents are growing smaller as the wave amplitude decays due to damping.

With this evidence, it is now appropriate to turn to some possible explanations.

5. Cylinder trajectories favorable to significant VIV

Recent work by Jauvtis and Williamson (2004) and Dahl and Triantafyllou (Dahl, 2008; Dahl et al., 2007) have provided evidence that the IL vibration of a rigid cylinder has an important influence on the CF lift forces and therefore CF response. IL response at twice ($2\times$) the CF response frequency has been shown to enable large CF response if the IL motion has an optimum phase angle with respect to the CF. Assume for the purpose of visualization that the CF motion (y-direction) and IL motion (x-direction) at any point on a rigid cylinder be described by the following equations:

$$\begin{aligned} y &= \sin(\omega t) \quad \text{Cross-flow response} \\ x &= 0.5\sin(2\omega t + \varphi) \quad \text{In-line response} \end{aligned} \tag{1}$$

The ratio of the amplitude of the IL to the CF motion has been arbitrarily chosen to be 0.5, a value typical of 2-D experiments. The phase angle (φ) determines the shape of the trajectory. Assume the flow past the cylinder is in the positive x direction. Then, referring to Fig. 9, it may be seen that the shape of the trajectories are controlled by the

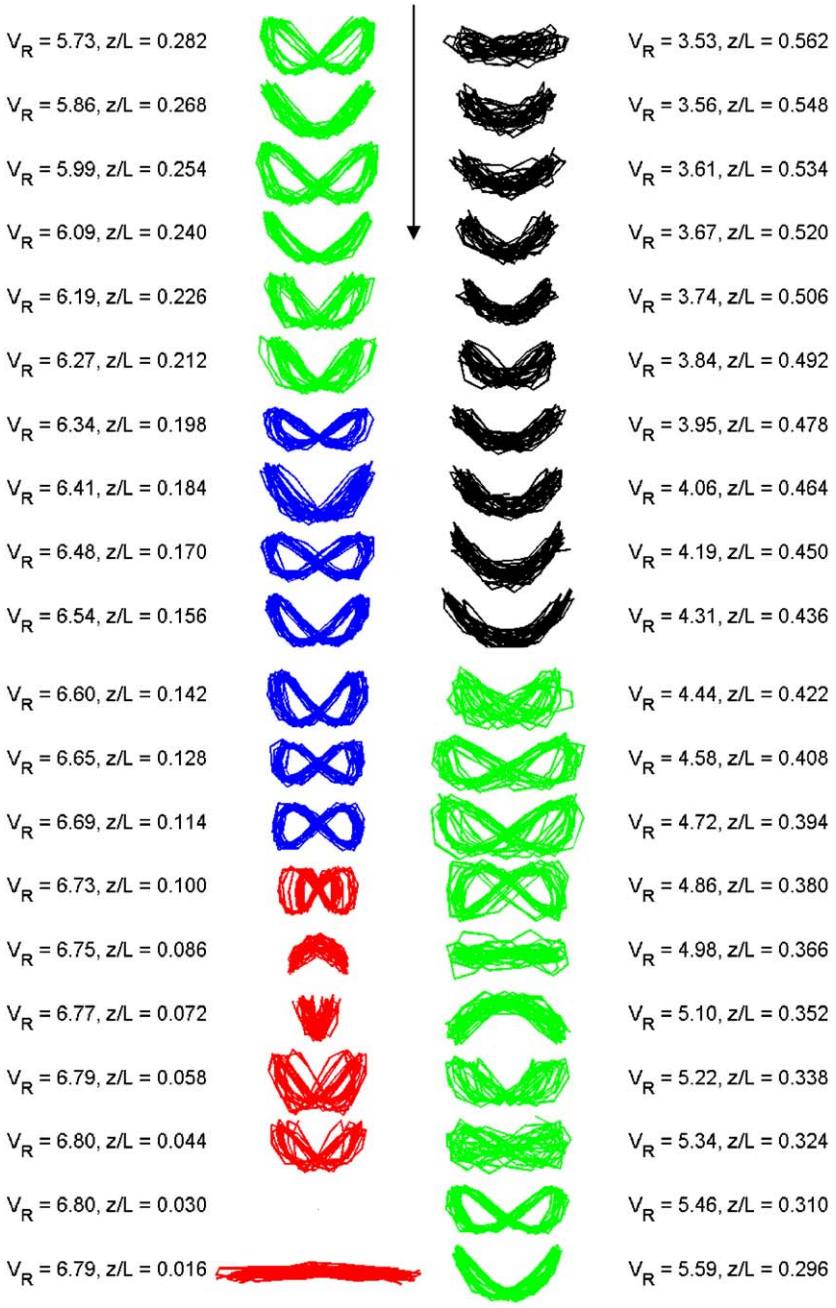

Fig. 8. Measured motion trajectories for the Miami II pipe from $z/L = 0.016$ to $z/L = 0.562$. The V_R estimates shown have a standard deviation of 0.20. The direction of the incident current is indicated by the arrow.

phase angle. In the figure the flow direction is down on the page. The trajectories in blue have phase angles that vary from 315° to 90°. For these phase angles the direction of the trajectory at the peaks in the CF motion are opposed to the flow. Dahl has shown that this range of phase angles is favorable for large amplitude VIV and leads to especially large $3\times$ lift forces. The optimum phase angle for $3\times$ lift forces is near 0°, when the trajectory is a figure eight and the motion is against the flow at the CF maxima. Dahl gives flow visualization evidence that at or near this phase

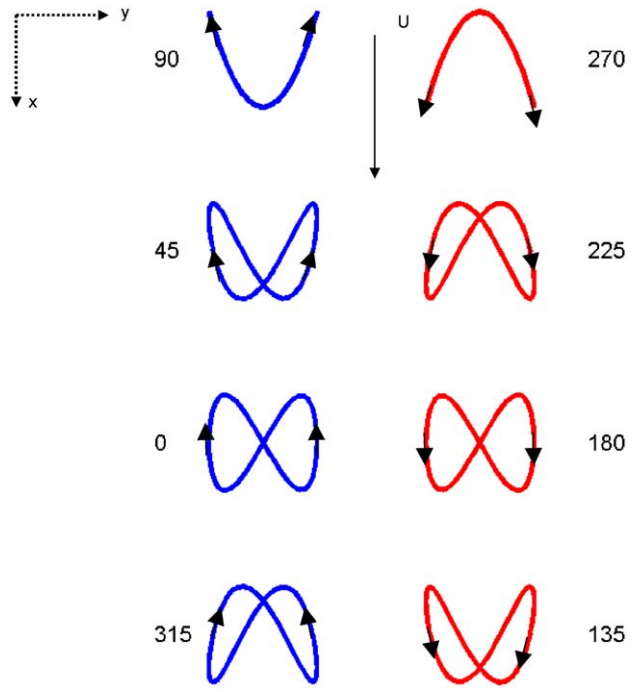

Fig. 9. Relationship between in-line and cross-flow motion phase angle (φ) and trajectories.

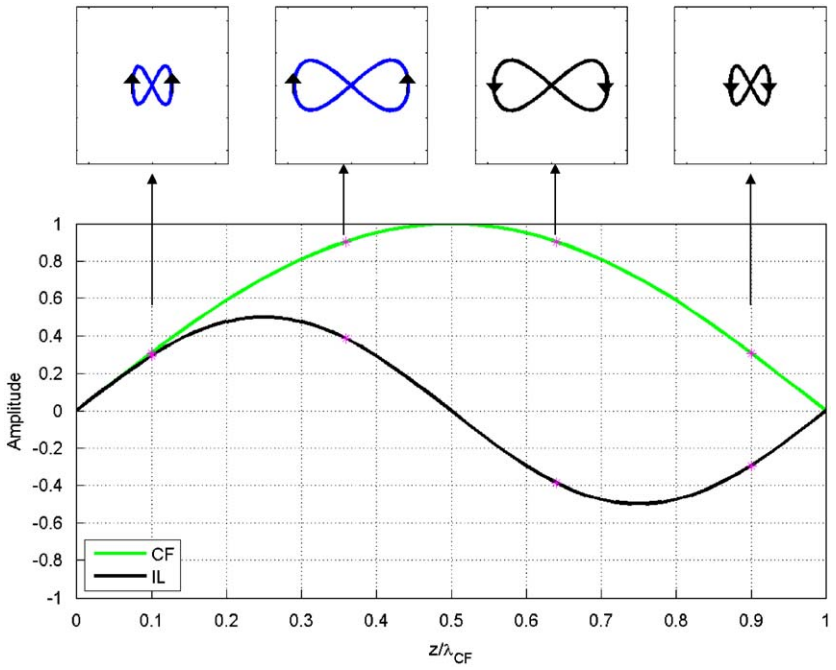

Fig. 10. Standing wave shapes for cross-flow (CF) and in-line (IL) motions and associated trajectories at different locations for a flexible cylinder with $\varphi = 0$.

angle the cylinder's downstream movement brings it close to recently shed vortices, thus enhancing the lift force. Also shown in this figure are phase angles from 135° to 270°. These trajectories are shown in red and are not favorable to significant VIV.

The Miami II test cylinder was tension dominated. This means that the velocity of traveling waves was independent of frequency. Therefore, the wavelength of 1X waves was twice that of $2\times$ waves. Fig. 10 depicts a $1\times$ and a $2\times$ standing wave. For the purpose of this example assume the phase angle (φ) is zero and the equations of these two waves are

$$y = A_1 \sin\left(\frac{2\pi z}{\lambda_1}\right)\sin(\omega_1 t) \quad \text{Cross-flow standing wave}$$
$$x = A_2 \sin\left(\frac{4\pi z}{\lambda_1}\right)\sin(2\omega_1 t + \varphi) \quad \text{In-line standing wave} \tag{2}$$

where the $1\times$ frequency is ω_1 and the $1\times$ wavelength is λ_1. By plotting x versus y motion as given in these equations the resulting trajectories will be figure eights (see Fig. 10) except at $z/L = 0$ and 1, where there is no motion and at 0.5 where the IL motion has zero amplitude and the CF is at a maximum resulting in a vertical line. Between 0 and 0.5, the trajectories are figure eights with the IL motion going against the flow at the CF peak amplitudes. Between 0.5 and 1.0, one will again see figure eights, but with the IL motion going with the flow at the CF extremes. Such standing waves would therefore be made up of alternating regions with favorable and unfavorable conditions supporting significant VIV. The net total VIV would be rather weak. This is supported by the observation that the measured standing wave region has lower amplitudes than expected and is only about 1.5 wavelengths long.

Now consider traveling waves on a tension dominated cylinder. The equations describing the IL(x) and CF(y) motions are given by

$$y = A_1 \sin\left(\frac{2\pi z}{\lambda_1} - \omega_1 t\right) \quad \text{Cross-flow traveling wave}$$
$$x = A_2 \sin\left(\frac{4\pi z}{\lambda_1} - 2\omega_1 t + \varphi\right) \quad \text{In-line traveling wave} \tag{3}$$

For the purpose of illustration, assume the phase angle (φ) is 0. Then if one picks any fixed position on the cylinder with a fixed value of z and constructs the x versus y trajectory plot as a function of time, the result is figure eight motions with the IL motion going against the flow at the extremes of the CF response. In other words, as long as the wave velocity remains constant, there would be a continuous length of cylinder in which the conditions are optimum for the formation of large amplitude IL and CF responses to VIV, including ideal conditions for the formation of the third harmonic CF forces.

With this information it becomes possible to explain the trajectories depicted in Fig. 8.

6. Insights about traveling waves on long cylinders

Fig. 8 is composed of four separate color coded regions. For each location, the trajectory of motion is shown as well as the reduced velocity (V_R) and z/L coordinate. The trajectories in red are in the standing wave region near the boundary. The trajectories in this region are consistent with standing waves because they change rapidly in shape with change in location. The first trajectory at $z/L = 0.016$ reveals mostly CF motion, because this is an anti-node for the CF motion and a node for the IL.

It has been explained that the standing wave region is weak, because at best it consists of alternating favorable and unfavorable VIV zones. Some standing wave region is inevitable because there will always be some waves traveling toward a boundary. These waves reflect at the pinned boundary condition and form a standing wave from the incident and reflected components. In the Miami tests this region was about 1.5 wavelengths long and soon gave over to traveling waves.

The second region in blue goes from $z/L = 0.10$ to 0.20. It reveals nearly constant figure eight trajectories of the kind that are favorable to VIV. This is a region of growth for the $3\times$, $4\times$ and $5\times$ components as revealed by the increasing rms amplitudes shown in Fig. 6. This region ends with a reduced velocity of approximately 6.3. The reduced velocity variation over this section of the pipe was from 6.3 to 6.7.

Fig. A1 in Appendix A provides a plot of reduced velocity of all harmonic components versus the rms strain for that component. This is for all pipe locations in which it was possible to isolate and obtain an estimate of the rms of each particular component. It is offered in this paper to stimulate thinking about the role of relationship, if any, of the reduced velocity and the higher harmonic components.

The third region in Fig. 8, depicted in green applies from $z/L = 0.21$ to 0.42. It reveals constantly changing trajectories, and yet is a region with traveling waves. The variation in trajectory shape means the IL and CF waves

are not staying phase locked to one another. This means that the IL and CF wave speeds are not remaining equal. This same region of the cylinder has a reduced velocity that is dropping from approximately 6.3 to 4.4. It is known from rigid cylinder laboratory tests that added mass for this sub-critical Reynolds number range also changes rapidly over this range of reduced velocities. A difference in added mass between the IL and CF vibrations would lead to different wave speeds and therefore changing trajectory patterns with distance traveled.

In the fourth region, colored black, the trajectories again settle down to a constant crescent shape, consistent with a phase angle of 90°. This persists over a long distance. The crescents become progressively smaller due to wave decay in this region. The reduced velocity variation is from 3.5 to 4.3.

The authors propose that the reason traveling waves dominate the VIV response is that on tension dominated cylinders traveling waves allow ideal phase angles and motion trajectories to exist over long lengths of the pipe. In contrast standing wave motion, at best, results in alternating regions which support or suppress large amplitude VIV. Therefore, standing wave regions are only weakly able to support VIV, compared to phase-locked traveling wave zones.

This may seem to contradict the observation of large figure eight motions observed at Castine, Maine in 1981, which were described in the Introduction. Castine was a very special case. The pipe was not tension dominated. The resonant IL mode was the fifth, the CF the third. Traveling waves were not favored because the entire pipe was only 1.5 wavelengths long. The $1\times$ and $2\times$ harmonic forces were all sufficient to drive the observed response.

7. Significance of bending stiffness on the higher harmonics

It has been shown that on a tension dominated cylinder, it is possible to have long regions with phase-locked IL and CF motions. Such phase-locked motion requires that the two waves travel at exactly the same speed, even though one is at twice the frequency of the other. If the two propagation speeds differ slightly, the phase between the two components will slowly diverge as the waves travel. If the wave speeds differ by only 5%, the phase angle will change by 90° in less than three wavelengths of the CF wave. An illustration of change in trajectories due to change in phase angle caused by different phase speeds in the CF and IL directions is shown in Fig. 11. This suggests that risers with bending stiffness which is sufficient to make wave propagation speeds only weakly frequency dependent, may not exhibit as much higher harmonic response. Strong $3\times$ and probably $5\times$ lift force components are associated with particularly favorable motion trajectories. If wave dispersion prevents substantial lengths of the riser from having phase locked $1\times$ (CF) and $2\times$ (IL) components then long regions of favorable traveling wave excitation will be prevented. Not only will there be much less higher harmonic fatigue damage, but the $1\times$ and $2\times$ response components may also be reduced, further reducing the fatigue damage rate.

Although the cylinder may have substantial bending stiffness, the added mass must also be taken into consideration. Even if the bending stiffness is enough to cause a 10% or 20% difference in wave speed, it is also possible that the

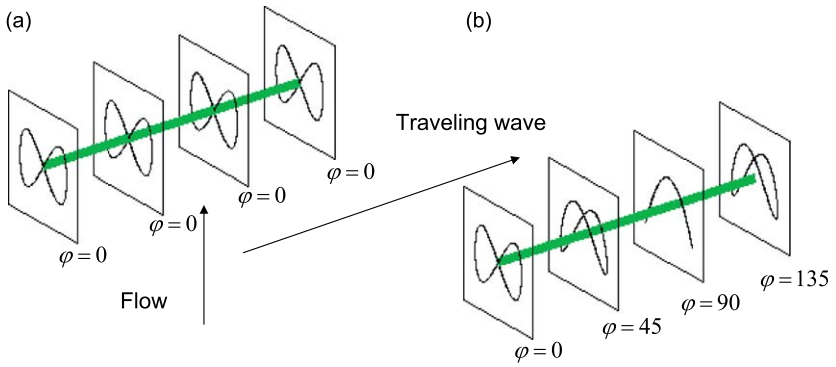

Fig. 11. Effect of cross-flow (CF) and in-line (IL) phase speeds on cylinder trajectories. (a) Equal phase speeds. (b) Unequal phase speeds. With equal CF and IL phase speeds, the phase angle (φ) and hence trajectories remain unchanged at different locations on pipe, while unequal CF and IL phase speeds lead to changing φ and consequently changing trajectories.

hydrodynamics of the wake may be able to self-adjust so as to keep the wave speed constant through an adjustment in the added mass. This is more likely to happen with low mass ratio cylinders, which are more sensitive to added mass variations.

8. Recommendations and conclusions

The Miami experiments have shown that traveling wave VIV is dominant at high mode numbers. The cylinder in these experiments was tension dominated, which favored long regions of wave propagation in which the IL and CF wave components traveled at the same speed. Thus traveling wave VIV excitation was favored. Future experiments are required to see if risers with sufficient bending stiffness to cause wave dispersion will reduce the VIV at the fundamental CF frequency and/or at the higher harmonics. In such experiments, the effects of added mass will have to be carefully observed.

The role of reduced velocity with traveling wave phenomena is likely to be very important. The experiments presented in this paper yielded some insight as to the role of reduced velocity, but more work needs to be done in that area, especially with respect to the relationship between reduced velocity and added mass and reduced velocity and the stability of phased locked traveling waves.

Acknowledgments

This research was sponsored by the DEEPSTAR Consortium, the Office of Naval Research Ocean Engineering and Marine Systems program (ONR 321OE), and the MIT SHEAR7 JIP.

Appendix A. Reduced velocity dependence of strain components

For all the strain components shown in Fig. A1, the reduced velocity was computed using the local current speed and the dominant 1X response frequency from the power-in region.

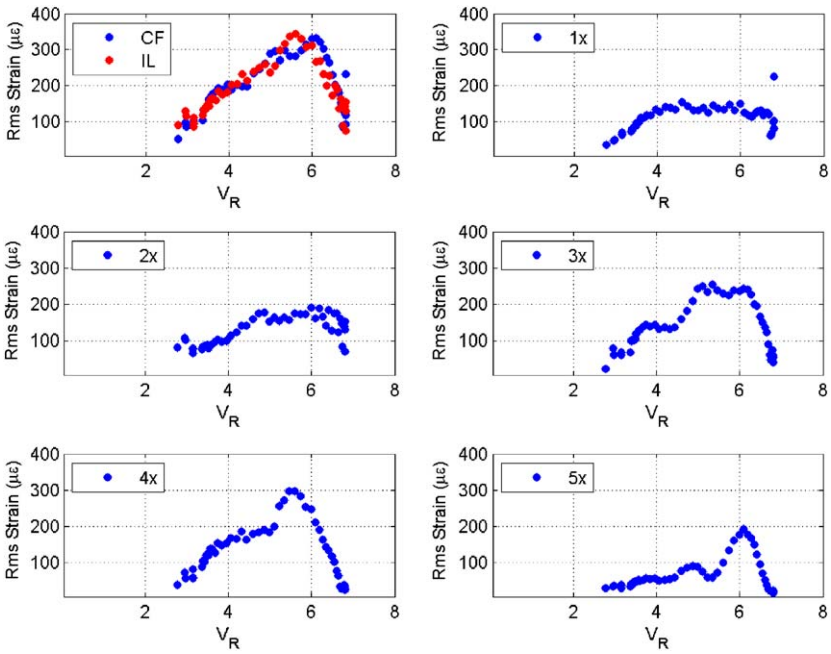

Fig. A1. Strain components versus reduced velocity.

References

Dahl, J.M., 2008. Vortex induced vibrations of a circular cylinder with combined in-line and cross-flow motions. Doctor of Philosophy Dissertation in Ocean Engineering, Department of Mechanical Engineering, Massachusetts Institute of Technology, Cambridge, MA, USA.

Dahl, J.M., Hover, F.S., Triantafyllou, M.S., Dong, S., Karniadakis, G.E., 2007. Resonant vibrations of bluff bodies cause multivortex shedding and high frequency forces. Physical Review Letters 99, 144503.

Jaiswal, V., Vandiver, J.K., 2007. VIV response prediction for long risers with variable damping. In: Proceedings of the 26th International Conference on Offshore Mechanics and Arctic Engineering, OMAE2007-29353.

Jauvtis, N., Williamson, C.H.K., 2004. The effect of two degrees of freedom on vortex-induced vibration at low mass and damping. Journal of Fluid Mechanics 509, 23–62.

Jhingran, V., 2008. Drag amplification and fatigue damage in vortex-induced vibration. Doctor of Philosophy Dissertation in Ocean Engineering, Prof. J.K. Vandiver, supervisor, Department of Mechanical Engineering, Massachusetts Institute of Technology, Cambridge, MA, USA.

Jhingran, V., Vandiver, J.K., 2007. Incorporating the higher harmonics in VIV fatigue predictions. In: Proceedings of the 26th International Conference on Offshore Mechanics and Arctic Engineering, OMAE2007-29352.

Marcollo, H., Chaurasia, H., Vandiver, J.K., 2007. Phenomena observed in VIV bare riser field tests. In: Proceedings of the 26th International Conference on Offshore Mechanics and Arctic Engineering, OMAE2007-29562.

Swithenbank, S., Vandiver, J.K., 2007. Identifying the power-in region for vortex-induced vibration on long flexible cylinders. In: Proceedings of the 26th International Conference on Offshore Mechanics and Arctic Engineering, OMAE2007-29156.

Vandiver, J.K., 1993. Dimensionless parameters important to the prediction of vortex-induced vibration of long, flexible cylinders in ocean currents. Journal of Fluids and Structures 7, 423–455.